DOI 10.48612/fpg/26nu-3hte-3n48

© *V. A. Glukhov**, *Yu. A. Goldin*, *G. V. Zhegulin*, *M. A. Rodionov*, 2022
© Translation from Russian: *E. S. Kochetkova*, 2022
Shirshov Institute of Oceanology, Russian Academy of Sciences, 117997, Nahimovsky Pr., 36, Moscow, Russia
*E-mail: vl.glukhov@inbox.ru

COMPLEX PROCESSING OF LIDAR SURVEY DATA OF MARINE AREAS

Received 30.03.2022; Revised 10.08.2022; Accepted 15.08.2022

The complex processing of data from the shipborne lidar survey of the Black Sea coastal areas was carried out. In this area, internal waves are often observed according to contact and satellite observations. The source of probing linearly polarized laser pulses in the lidar is a solid-state laser with diode pumping of the YAG: Nd active element with a pulse power of 20 mJ at a wavelength of 532 nm and a duration of 7 ns. The co- and cross-polarized components of the echo signal were recorded during the lidar survey. The cross-polarized component of the echo signal was mainly used due to its greater sensitivity to various kinds of inhomogeneities in the vertical distribution of hydrooptical characteristics. The purpose of processing is to identify quasi-periodic structures in the spatial distribution of the characteristics of lidar echo signals caused the propagation of short-period internal waves. Three processing methods were applied: the approximation method, the wavelet analysis method, and the Hilbert-Huang transform method. A large array of data obtained during 50 hours of lidar survey has been processed. Three 60-minute tracks containing quasi-periodic structures have been identified. The three processing methods results are in good agreement with each other and make it possible to obtain the most complete information about the parameters of the studied processes. The parameters of the recorded quasi-periodic processes are typical for internal waves observed in the coastal areas of the Black Sea. In the future, when processing a large amount of lidar sounding data, it is advisable to carry out fast processing by automated spectral methods at the first stage, and to carry out detailed processing by the approximation method only for those survey areas where quasi-periodic processes have been identified.

Keywords: shipboard polarized lidar, lidar survey, marine areas, internal waves, wavelet analysis, Hilbert-Huang transform

© *В. А. Глухов**, *Ю. А. Гольдин*, *Г. В. Жегулин*, *М. А. Родионов*, 2022
© Перевод с русского: *Е. С. Кочеткова*, 2022
Институт океанологии им. П.П. Ширшова РАН, 117997, Нахимовский пр., д. 36, г. Москва, Россия
*E-mail: vl.glukhov@inbox.ru

КОМПЛЕКСНАЯ ОБРАБОТКА ДАННЫХ ЛИДАРНОЙ СЪЕМКИ МОРСКИХ АКВАТОРИЙ

Статья поступила в редакцию 30.03.2022, после доработки 10.08.2022, принята в печать 15.08.2022

Выполнена комплексная обработка данных судовой лидарной съемки прибрежных районов Черного моря, в которых ранее с использованием контактных и спутниковых методов наблюдались короткопериодные внутренние волны. В качестве источника зондирующих линейно-поляризованных лазерных импульсов в лидаре использован твердотельный лазер с диодной накачкой активного элемента АИГ: Nd с импульсной мощностью 20 мДж на длине волны 532 нм и длительностью 7 нс. В ходе лидарной съемки регистрировались ко- и кросс-поляризованная компонента эхо-сигнала. При обработке использовалась в основном кросс-поляризованная компонента эхо-сигнала в силу её большей чувствительности к различного рода неоднородностям распределения гидрооптических характеристик с глубиной. Цель обработки — выявление квазипериодических структур в пространственном распределении характеристик лидарных эхо-сигналов, обусловленных распространением короткопериодных внутренних волн. В работе использовано три метода обработки: аппроксимационный метод, метод вейвлет-анализа и метод Гильберта-Хуанга. Обработан большой массив данных, полученных в результате 50 часов лидарной съемки. Выявлено три шестидесятиминутных трека, содержащих квазипериодические структуры. Результаты, полученные с использованием трех методов обработки, хорошо согласуются между собой и позволяют получить наиболее полную информацию о параметрах исследуемых

Ссылка для цитирования: *Глухов В.А.*, *Гольдин Ю.А.*, *Жегулин Г.В.*, *Родионов М.А.* Комплексная обработка данных лидарной съемки морских акваторий // Фундаментальная и прикладная гидрофизика. 2022. Т. 15, № 3. С. 27–42. doi:10.48612/fpg/26nu-3hte-3n48
For citation: *Glukhov V.A.*, *Goldin Yu.A.*, *Zhegulin G.V.*, *Rodionov M.A.* Complex Processing of Lidar Survey Data of Marine Areas. *Fundamental and Applied Hydrophysics.* 2022, 15, 3, 27–42. doi:10.48612/fpg/26nu-3hte-3n48

процессов. Параметры зарегистрированных квазипериодических процессов характерны для внутренних волн, наблюдаемых в прибрежных районах Черного моря. В дальнейшем при обработке большого объема данных лидарного зондирования целесообразно на первом этапе проводить быструю обработку автоматизированными спектральными методами, а детальную обработку аппроксимационным методом проводить только для тех участков съемки, на которых выявлены квазипериодические процессы.

Ключевые слова: судовой поляризационный лидар, лидарная съемка, морские акватории, внутренние волны, вейвлет-анализ, преобразование Гильберта-Хуанга

1. Introduction

Lidar survey of marine areas using radiometric lidars is efficient for the detection of light-scattering layers' parameters [1,2], fish schools, and position of high phytoplankton concentrations associated with blooms, including coccolithophorids [3–6]. Internal waves (IWs) determination and registration is a relevant application of lidar sounding [7–9]. The suitability of a lidar method for registering IWs is due to a correlation between the vertical distributions of hydrophysical and hydrooptical characteristics in subsurface layers of seawater. Because of this correlation, the remote estimation of the pycnocline depth is possible. Also, with the appropriate organization of the lidar survey process, it is practical to register quasi-periodic oscillations in the water column reflected in a change in the pycnocline position.

An important challenge of lidar sounding is the processing algorithms development and interpretation of both the result of each sounding and a series of results obtained when performing a lidar survey. A polarization processing algorithm estimates the stratification of a scattering coefficient based on the time dependence of the depolarization degree of the lidar echo signal [1, 3]. Various versions of the the base signal method compare the received echo signal shape with the echo signal shape for a homogeneous section of the underwater sounding path. This method has shown efficiency in dealing with subsurface scattering layers [3, 7, 10, 11]. The approximation method is an extension of the base signal method, which is applied successfully for boundary determination between layers with different hydrooptical characteristics in the case of two-layer stratification [9]. Tracking the position of a boundary between the layers during lidar sounding enables the registration of quasi-periodic structures caused by the IWs' propagation. To process a series of pulses obtained during a lidar sounding, we used spectral methods utilizing an amplitude change of the echo signal at a fixed depth. The comparison of processing results obtained with a range of methods is of particular interest because of the opportunity to derive a fuller insight into the studied process.

This work aims to use the complex processing of lidar survey data to register quasi-periodic processes occurring in the near-surface seawater and to determine their parameters.

2. Materials and methods

2.1. Description of equipment and methods of lidar survey

In this study we use the marine polarization lidar PLD-1 (jointly developed by the Laboratory of Ocean and Atmospheric Optics of the St. Petersburg Branch of the IO RAS and the Laboratory of Ocean Optics of the IO RAS) [12, 13]. As a source of probing pulses, the lidar uses a diode-pumped solid-state frequency-doubled YAG: Nd3+ laser (developed by LAGRAN LLC, Moscow) with the following characteristics: operating wavelength is 532 nm, probing pulse energy is 20 mJ, the probing pulse full width at half maximum is 7 ns, divergence at the 80 % energy level is 3 mrad, the probing radiation polarization is linear, and a repetition rate is 1 Hz.

The two-channel receiving system registers co- and cross-polarized components of the echo signal. The diameter of the receiving optical system of the co-polarized channel is 63 mm, the cross-polarized channel is 90 mm, and the field of view of the optical systems of both channels is 2°. The polarization method provides a number of advantages for the water column sounding with an inhomogeneous distribution of hydrooptical characteristics with depth [1, 2, 9, 13]. Therefore, in this work, we mainly analyse the cross-polarized component of the echo signal.

Signals from photodetectors are registered with a LeCroy HDO 4034 digital oscilloscope with a bandwidth of 350 MHz, a sampling rate of 2.5 GS/s, and a dynamic range of 12 bits. The vertical range resolution (the minimum change in the immersion depth of a scattering object detected by a lidar) is determined by the characteristics of the impulse function front of the measuring system. In the experiments with a moving flat shield, the PLD-1 lidar reliably recorded a range resolution of about 30 cm [12].

During the survey, the optical unit of the lidar was installed on the top deck of the vessel. The height of the the lidar above the water surface was 9.5 m. The lidar mounting and pointing device adjusted the probing angle to 20° from the vertical to minimize the influence of the specular reflection of the laser beam from the rough water surface.

The ranging method [14] that uses various parts of the signal with different sensitivities of the receiving-recording system allowed the expansion of the dynamic range of the lidar echo signals registration. One of the oscilloscope channels registered the entire signal range, from zero to the maximum amplitude; the other recorded the signal with a 10-fold amplification at the saturation of the impulse top. In this case, it is possible to record the echo signal attenuation curve at a depth of more than 10 m in more detail since the signal changes are considerably smaller than for the entire amplitude recording.

During the survey, the lidar was tacked at a low speed of 4 knots. Each of the lidar survey sessions lasted about 1 hour. From the drifting vessel between the series of lidar sounding, the light attenuation coefficient of seawater at a wavelength of 530 nm was measured with a C-Star Transmissometer with 25 cm path length, the C-Star Transmissometer was a part of Seabird SBE 25. The Secchi depth Z_S was estimated during daylight.

2.2. Conditions during experimental studies

Experimental studies took place in the Feodosia Bay of the Black Sea in the summer of 2016. The study area was located over the 1000–1200 m deep region near the continental slope from 100 to 1200 m. The contact observations [15, 16] and satellite imagery data [17–19] indicate that the shelf zone of the Black Sea is a place of active generation and propagation of IWs.

The Secchi depth Z_S in the area of experimental studies varied from 9 to 11 m. A typical profile of the vertical distribution of hydrophysical characteristics and the attenuation coefficient in the study area is shown in Figure 1. The total depth at the profile measurement point was 1050 m. The distribution features of the attenuation coefficient in this area are in good agreement with the distribution of hydrophysical characteristics. The layer of the increased gradient of the attenuation coefficient corresponds to the position of the pycnocline. It is important to note the complete absence of a layer of increased light scattering associated with the pycnocline.

Sea state did not exceed 1 point during the measurements. The vessel speed was 4 knots. The influence of surface waves and slight rolling on the accuracy of determining the position of the depth of the intermediate layer can be estimated using a long series of soundings of homogeneous areas. An analysis of similar sounding series showed that the layer boundaries error is 0.4 m. Lidar survey data were averaged over 20 signals during processing. The averaging reduced the multiplicative errors caused by the waves and ship motion to 0.2 m. Note that this averaging has practically no effect on the possibility of registering periodic structures in the period ranges of interest to 3–10 min.

2.3. Processing methods

The purpose of processing a lidar echo signals series is to search for and determine the parameters of quasi-periodic processes caused by the propagation of short-period IWs. The goal is to register the manifestation of quasi-periodic structures and determine the period, amplitude, timing, and a number of oscillations in a wave packet. Three methods were used to process the lidar survey data: the approximation method, the wavelet analysis, and the Hilbert-Huang transform. Each of the methods estimates the echo signal decay form and its changes in a series of lidar signals.

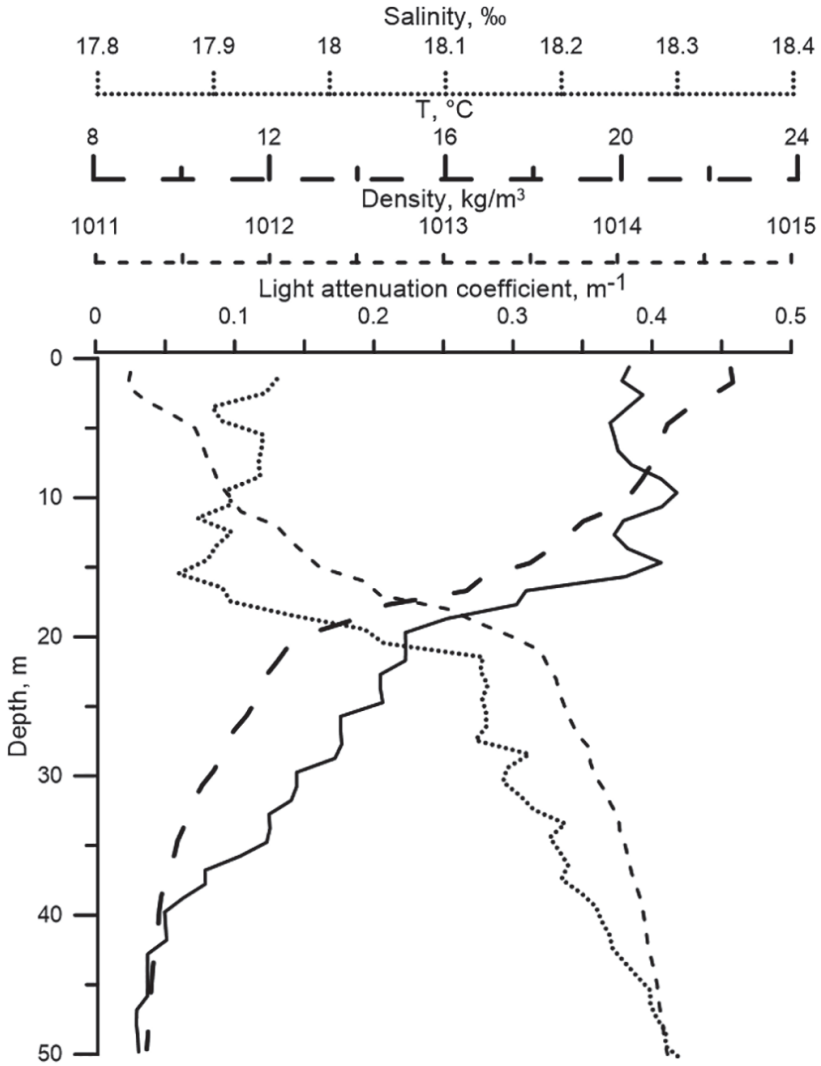

Fig. 1. Typical profile of the hydrophysical characteristics of sea water in the work region

Research [9] shows the efficiency of the approximation method for processing lidar signals with two-layer stratification of hydrooptical characteristics. The essence of the method is the identification of echo signal decay segments and tuning the parameters of the analytical approximation function, the form of which follows from the lidar equation [1]:

$$U(t) = a \cdot \frac{\exp(-b \cdot c_w t)}{(2n_w H + c_w t)^2},$$

where a and b are the approximation parameters, c_w is the speed of light in water, t is the time counted from the moment the probe pulse crosses the water surface, n_w is the refractive index of seawater, H is the distance from the lidar to the surface.

The shape of the echo signal attenuation with depth marked the segments' boundaries for approximation. The closeness of the segment approximations evaluated by a least square method determined the accuracy criterion for the depth intervals and parameters a and b. The intersection of the approximation curves for the upper and intermediate segments of the echo signal decay signal was a characteristic point. It marked the position of the boundary between the layers. As shown in [9], the position of the layer boundaries found by this method corresponds to the pycnocline location. The boundaries between the layers changed location under the influence of various hydrophysical factors changes with time. Remote registration of these changes was possible due to the processing of the lidar data array.

The advantage of this method is an image that shows the vertical displacement of the boundaries between layers attributed to the thermocline location, which allows estimation of the period, amplitude, number of oscillations in the train, and the time of registration of quasi-periodic structures. Presently the method is quite laborious since the existing processing program requires expert assessment to analyse each echo signal.

The other two methods used in this work are based on the spectral analysis of changes in the amplitudes of echo signals from a fixed depth, which carries information about the value of the backscatter coefficient. In this case, the problem of lidar data analysis is a search for quasi-periodic changes in the amplitude of the backscatter signal at given horizons.

Wavelet analysis is used for various problems in oceanology [20]. In particular, the parameters of the IWs were determined from the temperature profiles and the transmissometer [21] using wavelet analysis. This work also shows a high correlation between changes in temperature and the light attenuation coefficient of seawater in the region of the high gradient layer. Unlike the Fourier transform, wavelet analysis resolves both the presence of periodic processes in a given frequency interval as well as their allocation in time.

The wavelet analysis technique used to sample the amplitudes of lidar echo signals from a fixed depth is similar to the technique used to analyse thermal line data [21]. For the lidar sounding data pre-processing, the second-order Savitsky-Golay filtering of the initial signal was used with a window of 15 min to suppress low-frequency components comparable to the duration of the lidar sounding series [22]. The Morlet wavelet with a central frequency of 2π was chosen as the mother wavelet. For each sample from a given depth of the lidar series, the amplitudes of the wavelet transform coefficients and their significance levels were calculated in relation to Brownian noise with a 95 % threshold [23]. A disadvantage of wavelet analysis is the dependence of the accuracy of determining the parameters of quasi-periodic structures and their registration time on the duration and discreteness of measurements in a series of lidar soundings. The influence of edge effects and binding to a predetermined functional basis also introduces errors in the parameters of the selected signals.

Another method of spectral analysis is the Hilbert-Huang transform, which is actively used in various fields of science to study nonlinear and non-stationary oscillatory processes [24]. In oceanological applications [25–28], the Hilbert-Huang transform was used to study the parameters of nonlinear and collapsing IWs.

The Hilbert-Huang transform assumes that any signal consists of various internal types of oscillations superimposed on one another, and, in contrast to the Fourier analysis, the expansion is performed only for those harmonics (i. e., empirical modes) that are present in the original signal. Unlike harmonic analysis, where the signal model (discrete or continuous) is specified in advance, the empirical modes are determined during the processing. The method of empirical modes (EMD — Empirical Mode Decomposition) consisted of the decomposition of data into several internal mode functions (IMF — Intrinsic Mode Functions) and a trend function by sieving. Further, the Hilbert transform is applied to the IMF series to calculate the instantaneous frequency and amplitude of the signal for each moment in time. The Hilbert transform result is a series in three dimensions, signal duration, period, and amplitude. When analysing non-stationary processes, Hilbert spectra reflect energy flows in time, space, and between different components of the spectra also. The Hilbert-Huang transform allows tracking the frequency and amplitude change in time of the studied process.

The advantage of using the Hilbert-Huang transform over wavelet analysis is higher sensitivity to changes in the signal amplitude of the considered oscillatory process [27]. The decomposition of the original series is based on the signal itself and does not have a predetermined functional basis (unlike the wavelet transform), which means that it can be applied to signals of any shape. The Hilbert-Huang transform also does not require additional signal preparation, as in the case of wavelet analysis using the Savitsky-Golay filter.

Unlike the approximation method, which requires the participation of an operator and expert assessment, the processing of samples of lidar echo amplitudes at a given depth by spectral methods is fully automated. MATLAB 2021b software package with the built-in Signal Processing Toolbox and Wavelet Toolbox functions was used for the software implementation of the spectral methods.

3. Results and discussion

The total time of the lidar survey was about 50 hours. After a large amount of data processing, three tracks with quasi-periodic structures were identified. Figures 2–5 show the results of processing the lidar survey data on track No. 1. The approximation method results are shown in Figure 2. The upper curve corresponds to the upper boundary of the intermediate layer, and the lower curve denotes the lower one. For echo signals at the beginning of the cycle, considering the features of the decay shape, the following depth intervals were chosen for the parameters of the approximating functions: 11–13 m, 13–16 m, and 16–21 m. In the event of the echo signal shape change during processing, the position of these boundaries is corrected. The result of the track processing shows that the position of the upper boundary of the layer remains practically constant throughout the entire track, while a clearly pronounced periodic structure is recorded at the lower boundary. The average oscillation period was 5 min, and the amplitude was about 1 m.

Wavelet analysis of the track No. 1 data was performed for the time-dependent change in the amplitudes of the echo signal at a fixed depth in the range of 14–24 m with a step of 1 m. The clearest result was obtained for a depth of 17 m, close to the position of the thermocline. The result of the wavelet analysis of this horizon is shown in Figure 3. In Figure 3, *a*, the local coefficients of the wavelet transform are presented in graphical form, the abscissa is the time axis for lidar echo signal series, and the ordinate axis is the period. Figure 3, *a* is a wavelet image showing all the characteristic features of the process, the scale and intensity of periodic changes in the amplitude of the lidar echo signal at a given depth, as well as the presence, location, and duration of areas

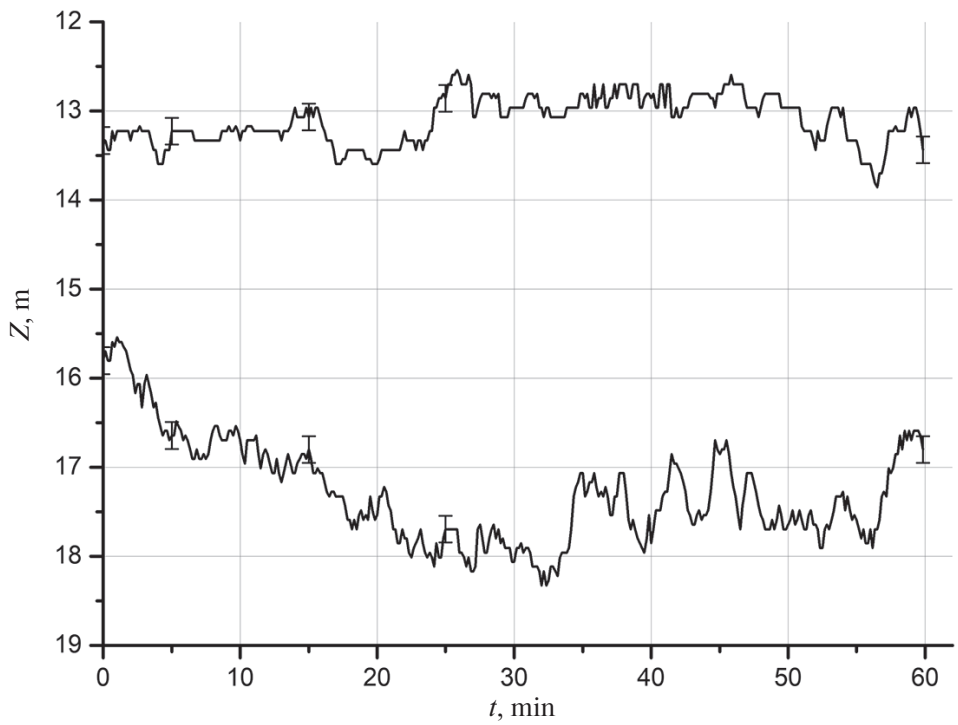

Fig. 2. The position of the upper and lower boundaries of the middle layer, obtained on the track No. 1 by the approximation method

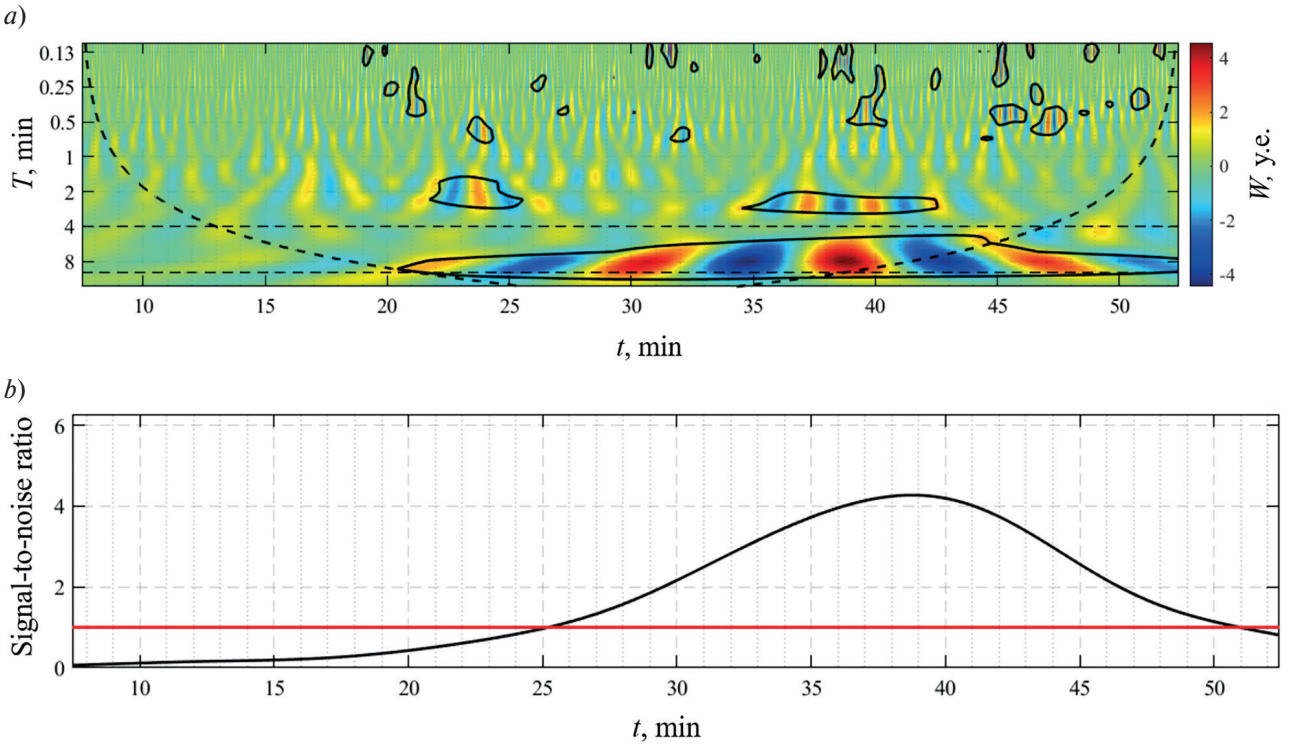

Fig. 3. The result of data processing of the track No. 1 from a fixed depth of 17 m using wavelet analysis: *a* — the amplitudes of the wavelet transform coefficients; *b* — the time-averaged power of the wavelet spectrum, normalized to the 95% significance level with respect to the Brownian noise

corresponding to increased values of the wavelet coefficients. The solid black line marks statistically significant parts of the signal having a 95% significance level compared to Brownian noise. In the lower right part of the figure, there is a statistically significant signal segment with a central period of 6 min and a duration of about 30 min, which indicates the presence of a quasi-periodic process with the corresponding characteristics, detected by an amplitude change of lidar echo signals at a specific depth.

The dotted curve highlights the zone of strong edge effects. The range of periods indicated in the figure is determined from the expression for the time scales of the signal and depends on the discreteness and duration of the original signal [23]. In Fig 3 the dashed horizontal lines show the time ranges for the power of the wavelet spectrum averaging. The spectral power of Brownian noise is presented as unity. From the 25th to the 50th minute, the values of the averaged power spectrum exceed the Brownian noise power, which confirms the significance of fluctuations in this time interval.

The result of wavelet analysis of data from the same track, but obtained from a depth of 14 m, is shown in Fig 4. Oscillations in the considered range of periods also find a place at this depth, but the calculation of the power spectrum averaged over time scales from 4 to 8 min, shown in Figure 4, b, makes it possible to estimate the significance of these oscillations. For almost the entire track, the average power spectrum is less than unity, which indicates that these signals are insignificant despite the periodicity. This result is consistent with the behaviour of the upper boundary of the intermediate layer, the position of which was obtained using the approximation method (Fig 2).

The data of track No. 1 were also processed using The Hilbert-Huang transform. Figure 5 shows the spectrum calculated for the amplitudes of lidar echo signals at a depth of 17 m. The figure shows the time behaviour of the IMF for time ranges of 1–8 min. The amplitude of the presented mode function is shown in colour. The dimension of the amplitude coincides with the dimension of the original sample from the depth. A wave packet is observed in the spectrum with a 2–5 min period and a duration of about 30 min.

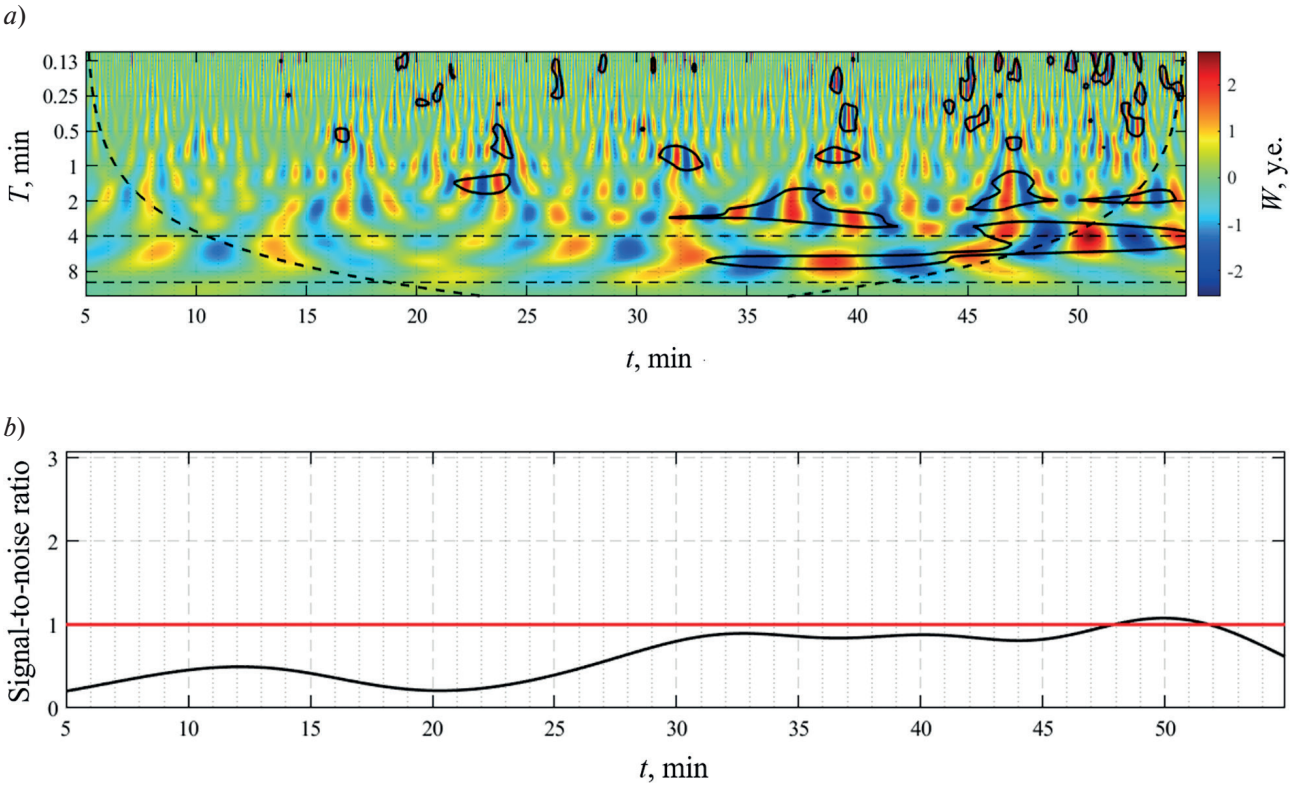

Fig. 4. The result of data processing of the track No. 1 from a fixed depth of 14 m using wavelet analysis: *a* — the amplitudes of the wavelet transform coefficients; *b* — the time-averaged power of the wavelet spectrum, normalized to the 95% significance level with respect to the Brownian noise

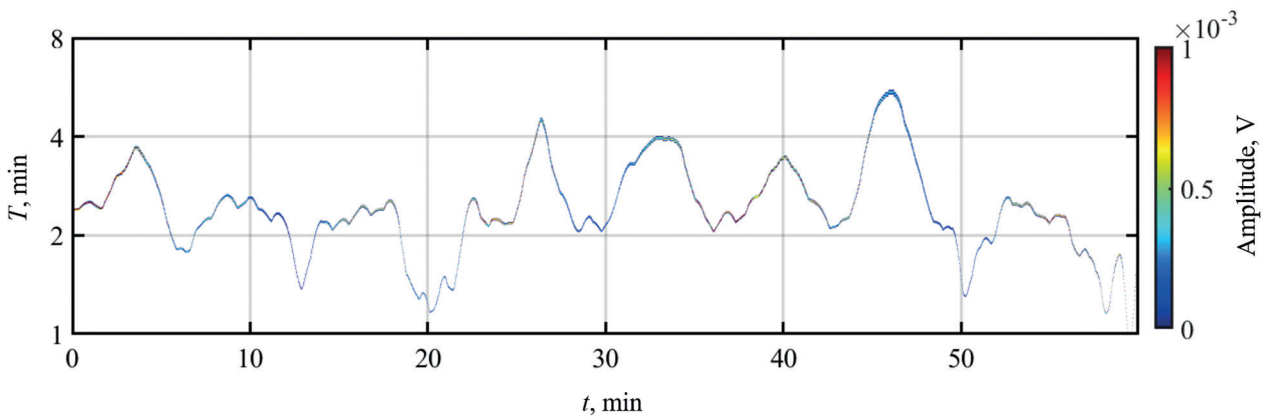

Fig. 5. The intrinsic mode function, characterized by periods from 1 to 8 min, obtained by processing the distribution of echo signal amplitudes from the depth of 17 m on track No. 1 using the Hilbert-Huang transform

The results of No. 2 track processing are shown in Figures 6–8. The approximation method for the track is shown in Figure 6. For the echo signals at the beginning of the cycle, the following depth intervals were chosen for the approximating functions parameters' evaluation: 11–13, 13–16, and 16–21 m. Dissimilar to track No. 1, synchronous oscillations of the upper and lower boundaries of the intermediate layer were recorded. The maximum amplitude at the upper boundary was 1 m, and 2 m at the lower boundary. In total, 5 oscillations are observed with an average period of 8 min.

For the track No. 2 data, wavelet analysis was performed for the echo signal amplitude change with time at a fixed depth in the range of 14–24 m with a step of 1 m. The most evident result was obtained for a depth of 18 m. Figure 7 shows an analysis at this horizon. Statistically significant fluctuations with a period lying in the range of 4–8 min throughout almost the entire track are identified with the wavelet analysis.

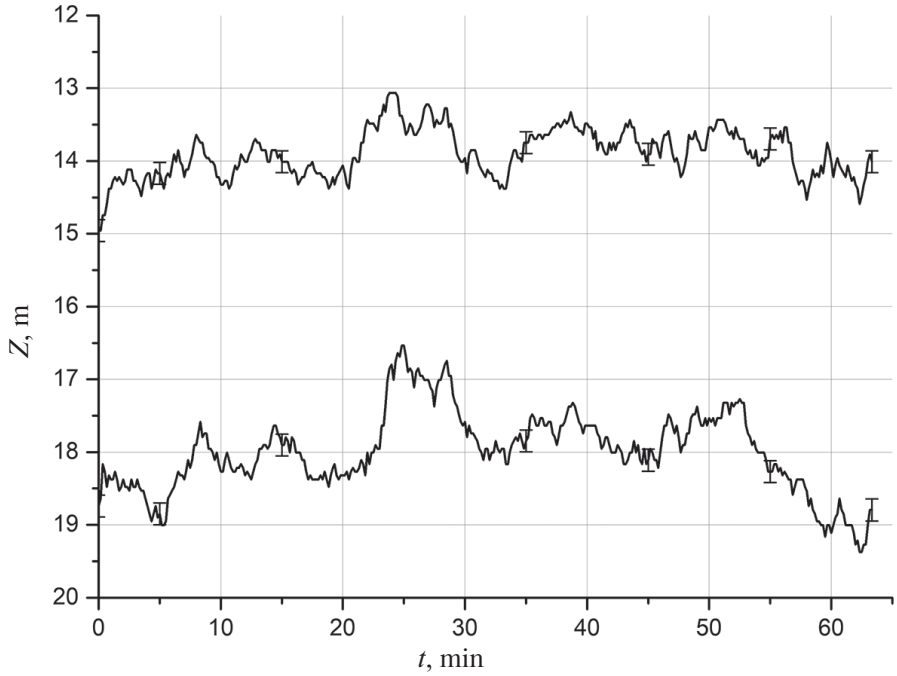

Fig. 6. The position of the upper and lower boundaries of the middle layer, obtained on the track No. 2 by the approximation method

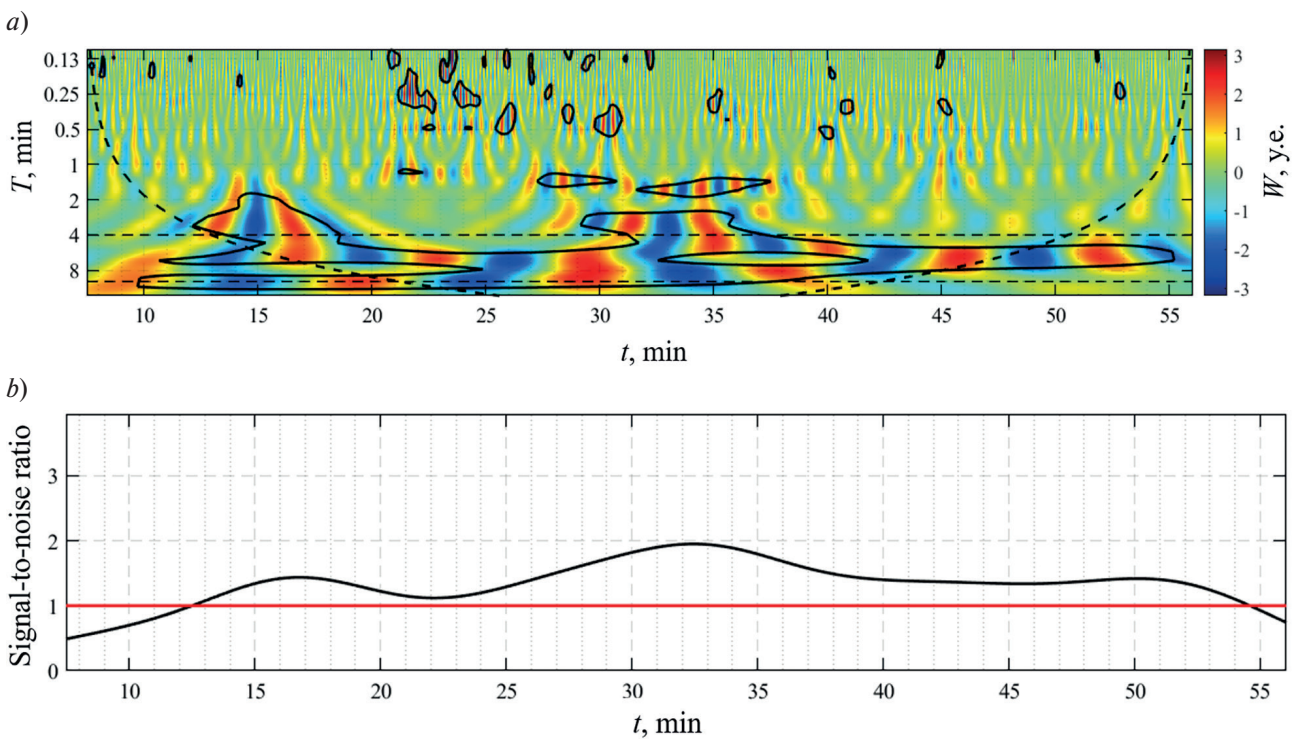

Fig. 7. The result of data processing of the track No. 2 from a fixed depth of 18 m using wavelet analysis: *a* — the amplitudes of the wavelet transform coefficients; *b* — the time-averaged power of the wavelet spectrum, normalized to the 95% significance level with respect to the Brownian noise

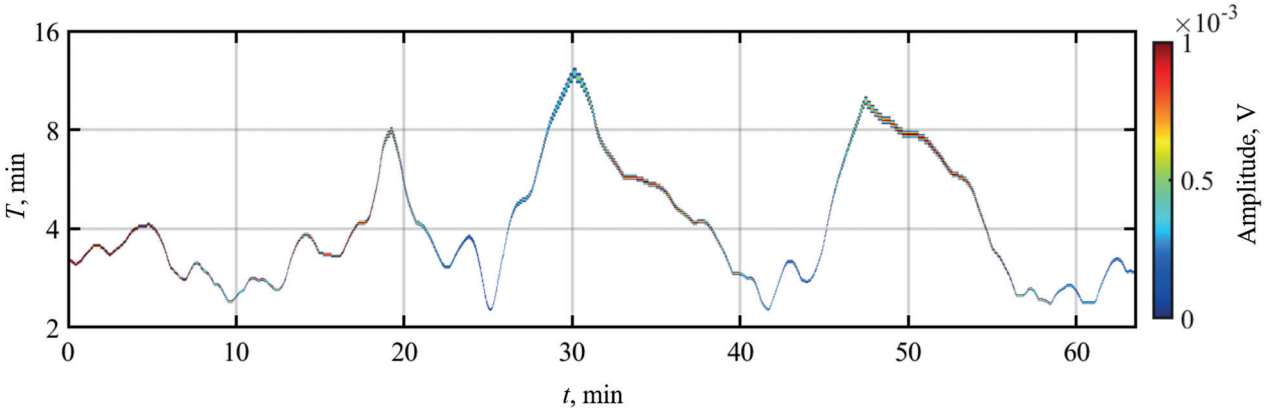

Fig. 8. The intrinsic mode function, characterized by periods from 2 to 16 min, obtained by processing the distribution of echo signal amplitudes from a depth of 18 m on track No. 2 using the Hilbert-Huang transform

Tack No. 2 processing results from a horizon of 18 m by the Hilbert-Huang transform are shown in Figure 8. The figure shows the IMF behaviour in time for periods of 2–16 min. The spectrum reveals a wave packet of three oscillations with periods between 2 and 12 min. Unlike the approximation method, the Hilbert-Huang transform precisely identified periodic structures starting from the 15th minute. This can be explained by the fact that the approximation method determined the first two oscillations; however, due to the considerable difference in the period (about 5 minutes) with the following oscillations, the harmonics did not fit the expansion of the IMF and remained undetected.

The track No. 3 processing results are shown in Figures 9–11. Figure 9 shows the approximation method performance. For the echo signals at the beginning of the cycle, the following depth intervals were chosen for approximating functions parameters estimation, 11–13, 13–16, and 16–21 m.

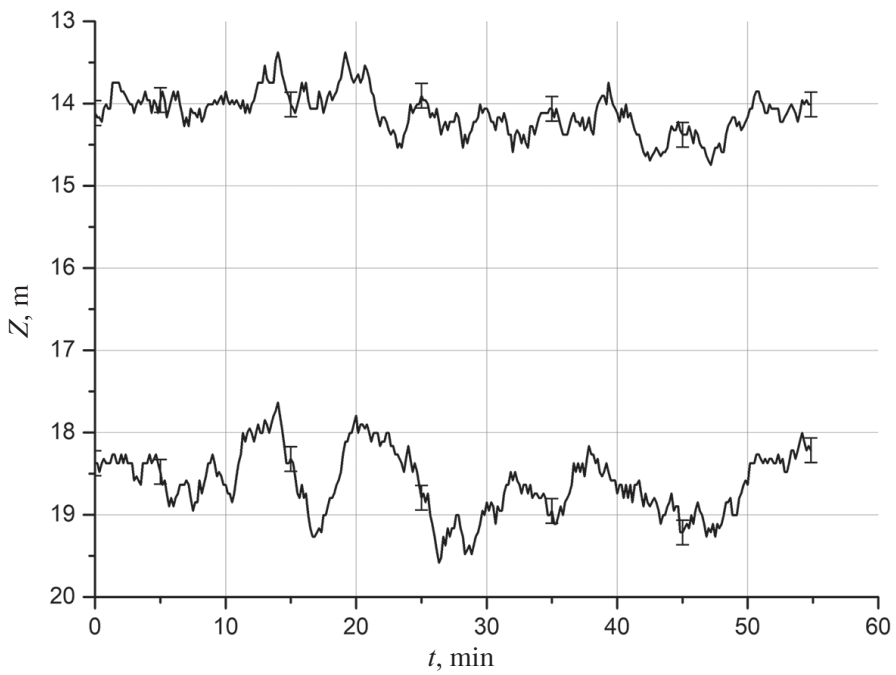

Fig. 9. The position of the upper and lower boundaries of the middle layer, obtained on the track No. 3 by the approximation method

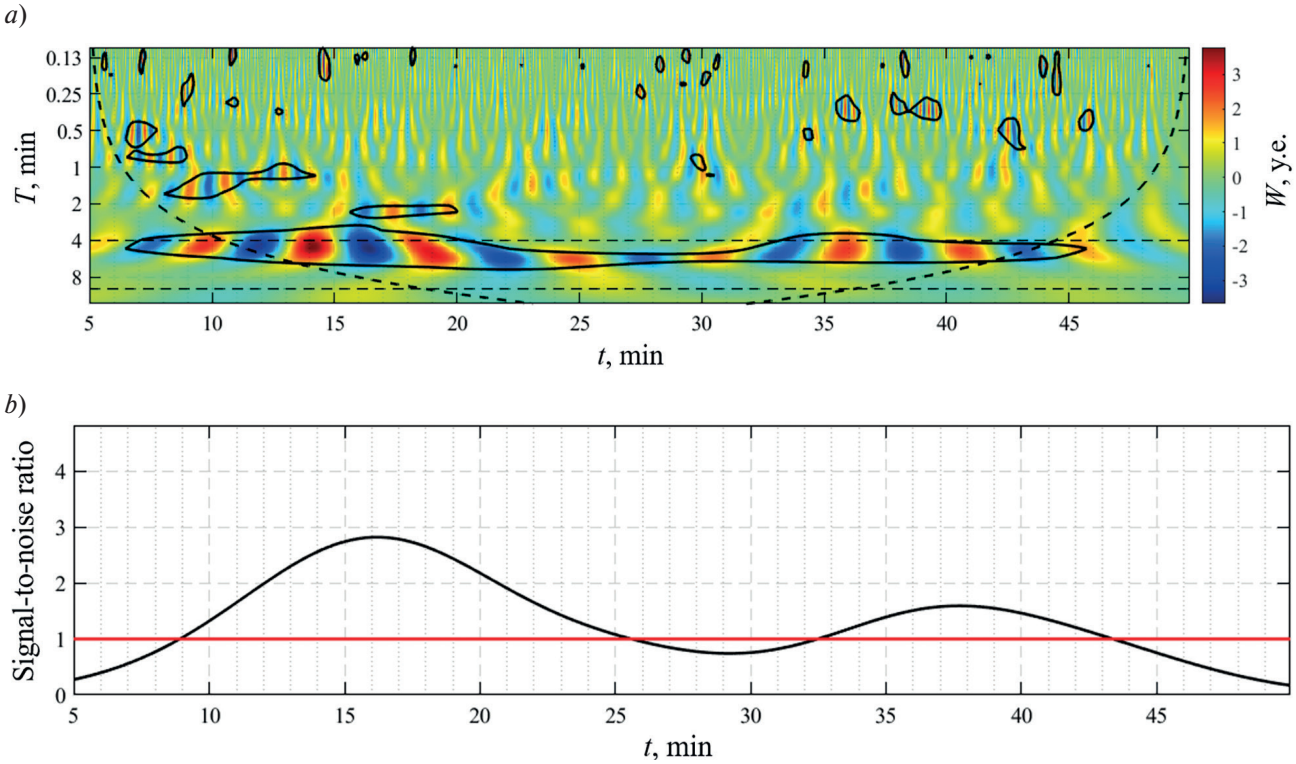

Fig. 10. The result of data processing of the track No. 3 from a fixed depth of 18 m using wavelet analysis: *a* — the amplitudes of the wavelet transform coefficients; *b* — the time-averaged power of the wavelet spectrum, normalized to the 95% significance level with respect to the Brownian noise

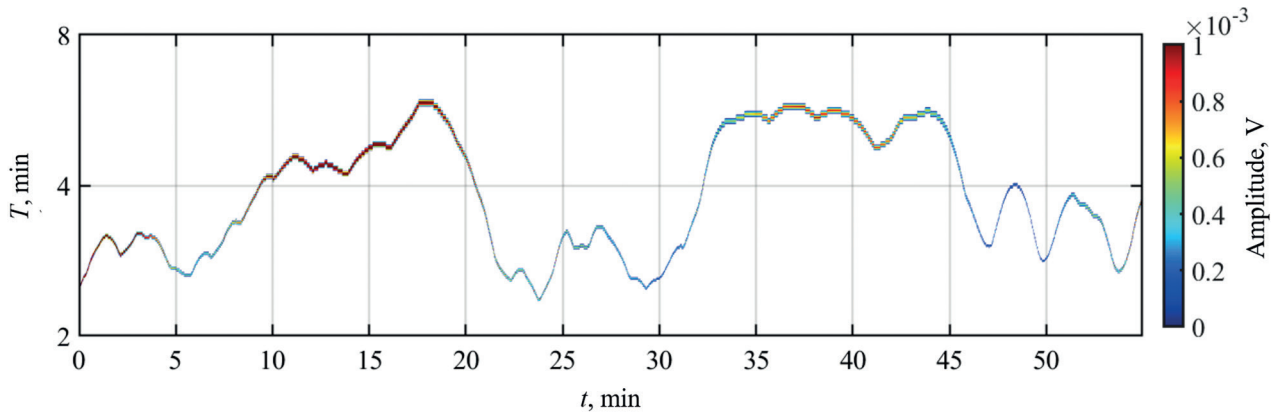

Fig. 11. The intrinsic mode function, characterized by periods from 2 to 8 min, obtained by processing the distribution of echo signal amplitudes from a depth of 18 m on track No. 3 using the Hilbert-Huang transform

Note that four oscillations are distinguished at the lower boundary, while only the two most intense fluctuations are traced at the upper boundary. The maximum amplitude at the upper boundary is 0.6 m, and 2 m at the lower boundary. The average oscillation period is 7 min.

Similar to the track No. 2, the most considerable result obtained with the wavelet analysis at the track No. 3 was for a depth of 18 m. The results are shown in Figure 10. Periodic structures were registered throughout almost the entire track. The most intense oscillations were observed in the first half of the track, which agrees with the approximation method result.

Figure 11 shows the Hilbert-Huang spectrum obtained for a depth of 18 m. Apparently, oscillations with an average period of 6–7 min are detected in the spectrum along the track. In this case, the most intense oscillations are observed in the first half of the track, which is shown in colour in Figure 11 and in agreement with the results shown in Figures 9 and 10.

The IWs were registered while the vessel was on the move at a speed of 4 knots (2 m/s). Using the hydrological measurements in the research area, the estimate of the IWs' phase velocity was 0.5 m/s. However, the internal waves' propagation direction was not determined during the experiment. Therefore, only the interval limits of measured wavelength were estimated for the measured IWs with a 6 min period. It was 540 m when the vessel was moving against the wave and 900 m when the directions coincided. To estimate the real value of the IW's wavelength, the angle between the velocities of the vessel is necessary, but it belongs to this interval.

The results obtained using spectral methods for all three tracks, namely the period and localization of quasi-periodic structures, are in good agreement with each other and with the result obtained by the approximation method. Some discrepancies in the position and periods of the selected oscillations are due to non-strict periodicity and a limited number of periods, which complicate the spectral analysis.

4. Conclusion

The performed complex processing of the data array from the shipborne lidar survey in the Black Sea coastal areas was aimed at searching for and determining the parameters of quasi-periodic structures caused by the propagation of IWs. The three processing methods were used. Each of the methods has its advantages and disadvantages. The most illustrative is the approximation method, which provides an image of vertical displacements of regions with sharp gradients of the attenuation coefficient confined to the density gradient layer. The advantage of the applied spectral methods, namely, wavelet analysis and the Hilbert-Huang transform, is the possibility of fast processing of a large data array, which produces an estimation of the period and localization of quasi-periodic processes. The results obtained by each of the three methods are generally consistent with each other. Some quantitative discrepancies may be due to the non-strict periodicity of the processes under study and the limited number of fluctuations in a train, which complicate the spectral analysis. Presently, the approximation method requires an expert assessment, which makes its application very laborious. Therefore, when processing large data arrays, it is advisable at the first stage to perform fast automated spectral approaches and proceed to detailed processing by the approximation method only for those survey areas where quasi-periodic processes were identified. This approach significantly facilitates the retrieval of the fullest information.

The methods described in this work can be applied to airborne lidar survey data, which has a number of advantages, such as high productivity and the ability to obtain a synoptic picture of the dynamic processes occurring in the near-surface layer of seawater. For the following steps, it is necessary to conduct studies in waters with other types of stratification, while lidar sounding should be complemented by synchronous contact measurements of hydrophysical and hydrooptical characteristics.

Funding

Experimental studies and processing of the registered data array by spectral methods were carried out as part of the state assignment No. FMWE-2021–0014. The processing of the registered data array by the approximation method was carried out with the financial support of the Ministry of Education and Science of the Russian Federation, project No. 075–15–2021–934 (The study of anthropogenic and natural factors of changes in the composition of air and environmental objects in Siberia and the Russian sector of the Arctic in conditions of rapid climate change using the Tu-134 Optik flying laboratory).

References

1. *Vasilkov A.P.*, *Goldin Yu.A.*, *Gureev B.A.*, *Hoge F.E.*, *Swift R.N.*, *and Wright C.W.* Airborne polarized lidar detection of scattering layers in the ocean. *Applied Optics*. 2001, 40, 4353–4364. doi:10.1364/AO.40.004353
2. *Churnside J.H.*, *Donaghay P.L.* Thin scattering layers observed by airborne lidar. ICES *Journal of Marine Science*. 2009, 66(4), 778–789. doi:10.1093/icesjms/fsp029
3. *Collister B.L.*, *Zimmerman R.C.*, *Hill V.J.*, *Sukenik C.I.*, *Balch W.M.* Polarized lidar and ocean particles: insights from a mesoscale coccolithophore bloom. *Applied Optics*. 2020, 59(15), 4650–4662. doi:10.1364/AO.389845
4. *Churnside J.H.*, *Brown E.D.*, *Parker-Stetter S.*, *Horne J.K.*, *Hunt G.L.*, *Hillgruber N.*, *Sigler M.F.*, *Vollenweider J.J.* Airborne remote sensing of a biological hot spot in the southeastern Bering Sea. *Remote Sensing*. 2011, 3(3), 621–637. doi:10.3390/rs3030621
5. *Goldin Y.A.*, *Vasilev A.N.*, *Lisovskiy A.S.*, *Chernook V.I.* Results of Barents Sea airborne lidar survey. *Proceedings SPIE. Current Research on Remote Sensing*, *Laser Probing*, *and Imagery in Natural Waters* (*13 April 2007*). 2007, 6615E, 126–136. doi:10.1117/12.740456
6. *Zhong C.*, *Chen P.*, *Pan D.* An improved adaptive subsurface phytoplankton layer detection method for ocean lidar data. *Remote Sensing*. 2021, 13(19), 3875. doi:10.3390/rs13193875
7. *Churnside J.H.*, *Ostrovsky L.A.* Lidar observation of a strongly nonlinear internal wave train in the Gulf of Alaska. *International Journal of Remote Sensing*. 2005, 26(1), 167–177. doi:10.1080/01431160410001735076
8. *Bukin O.A.*, *Major A.Y.*, *Pavlov A.N.*, *Shevtsov B.M.*, *Kholodkevich E.D.* Measurement of the lightscattering layers structure and detection of the dynamic processes in the upper ocean layer by shipborne lidar. *International Journal of Remote Sensing*. 1998, 19(4), 707–715. doi:10.1080/014311698215946
9. *Glukhov V.A.*, *Goldin Yu.A.*, *Rodionov M.A.* Method of internal waves registration by lidar sounding in case of waters with two-layer stratification of hydrooptical characteristics. *Fundamental and Applied Hydrophysics*. 2021, 14(3), 86–97 (In Russian). doi:10.7868/S2073667321030084
10. *Hoge F.E.*, *Wright C.W.*, *Krabill W.B.*, *Buntzen R.R.*, *Gilbert G.D.*, *Swift R.N.*, *Berry R.E.* Airborne lidar detection of subsurface oceanic scattering layers. *Applied Optics*. 1988, 27(19), 3969–3977. doi:10.1364/AO.27.003969
11. *Goldin Y.A.*, *Gureev B.A.*, *Ventskut Y.I.* Shipboard polarized lidar for seawater column sounding. *Proccedings SPIE. Current Research on Remote Sensing*, *Laser Probing*, *and Imagery in Natural Waters* (*13 April 2007*). 2007, 6615, 152–159. doi:10.1117/12.740466
12. *Goldin Yu.A.*, *Rodionov M.A.*, *Gureev B.A.*, *Glukhov V.A.* Marine polarization lidar PLD-1. *Proceedings of XIII All-Russian Conference* "*Advanced Technologies of Hydroacoustics and Hydrophysics*" (*St. Petersburg*, *2016*). St. Petersburg, Saint-Petersburg Research Center of RAS, 2016, 215–217 (In Russian).
13. *Glukhov V.A.*, *Goldin Yu.A.*, *Rodionov M.A.* Experimental estimation of the capabilities of the lidar PLD-1 for the registration of various hydro-optical irregularities of the sea water column. *Fundamental and Applied Hydrophysics*. 2017, 10(2), 41–48 (In Russian). doi:10.7868/S207366731702006X
14. *Goldin Yu.A.*, *Rogozkin D.B.*, *Sheberstov S.V.* Polarized lidar sounding of stratified seawater. *Proceedings of IV International Conference* "*Current Problems in Optics of Natural Waters* (*ONW'2007*)". Nizhny Novgorod, 2007, 175–178.
15. *Khimchenko E.E.*, *Serebryany A.N.* Internal waves on the Caucasian and Crimean shelves of the Black Sea (according to summer-autumn observations 2011–2016). *Journal of Oceanological Research*. 2018, 46(2), 69–87 (In Russian). doi:10.29006/1564–2291.JOR-2018.46(2).7
16. *Serebryany A.N.*, *Ivanov V.A.* Study of internal waves in the Black Sea from oceanography platform of Marine Hydrophysical Institute. *Fundamental and Applied Hydrophysics*. 2013, 3, 34–45 (In Russian).
17. *Zimin A.V.*, *Svergun E.I.* Analysis of the characteristics and assessment of the expected heights of internal waves on the Crimean shelf according to the expedition data in the summer of 2016. *Proceedings of the Russian Scientific and Practical Conference* "*IV Feodosia Scientific Readings*" (St. Petersburg, September 11–12, 2017). Feodosia, Art-Life, 230–234 (in Russian).
18. *Lavrova O.Y.*, *Serebryany A.N.*, *Mityagina M.I.*, *Bocharova T.Y.* Subsatellite observations of small-scale hydrodynamic processes in the northeastern Black Sea. *Sovremennye Problemy Distantsionnogo Zondirovaniya Zemli iz Kosmosa*. 2013, 10(4), 308–322 (in Russian).

19. *Ivanov V.A.*, *Shul'ga T. Ya.*, *Bagaev A.V.*, *Medvedeva A.V.*, *Plastun T.V.*, *Verzhevskaia L.V.*, *Svishcheva I.A.* Internal waves on the Black Sea shelf near the Heracles Peninsula: Modeling and observation. *Physical Oceanography*. 2019, 26(4), 288–304. doi:10.22449/1573-160X-2019-4-288-304
20. *Astaf'eva N.M.* Wavelet analysis: basic theory and some applications. *Physics-Uspekhi*. 1996, 39(11), 1085. doi:10.1070/PU1996v039n11ABEH000177
21. *Zhegulin G.V.* Using wavelet analysis to assess the relationship of hydrological and hydrooptical oscillations in the range of internal waves according to in situ observations in the White Sea. *Fundamental and Applied Hydrophysics*. 2016, 9(3), 48–56 (in Russian).
22. *Press W.H.*, *Teukolsky S.A.* Savitzky–Golay smoothing filters. *Computers in Physics*. 1990, 4(6), 669–672. doi:10.1063/1.4822961
23. *Koronovskiy A.A.*, *Khramov A.E.* Continuous wavelet analysis and its applications. *Moscow*, *FIZMATLIT*, 2003. 176 p. (in Russian).
24. *Huang N.E.*, *Wu Z.* A review on Hilbert-Huang transform: Method and its applications to geophysical studies. *Reviews of Geophysics*. 2008, 46(2). doi:10.1029/2007RG000228
25. *Navrotsky V.V.* et al. Internal waves and mixing in the shelf zone of the sea. *Izvestia TINRO* (Pacific Research Fisheries Center). 2010, 162, 324–337 (in Russian).
26. *Navrotsky V.V.*, *Lobanov V.B.*, *Sergeev A.F.*, *Voronin A.A.*, *Gorin I.I.*, *Pavlova E.P.* Dynamic structure of cascading in the Peter the Great Bay (Sea of Japan). *Oceanological Research*. 2020, 48(3), 148–163 (in Russian). doi:10.29006/1564–2291.JOR-2020.48(3).9
27. *Dätig M.*, *Schlurmann T.* Performance and limitations of the Hilbert–Huang transformation (HHT) with an application to irregular water wave. *Ocean Engineering*. 2004, 31(14–15), 1783–1834. doi:10.1016/j.oceaneng.2004.03.007
28. *Ezer T.*, *Heyman W.D.*, *Houser C.*, *Kjerfve B.* Modeling and observations of high-frequency flow variability and internal waves at a Caribbean reef spawning aggregation site. *Ocean Dynamics*. 2010, 61(5), 581–598. doi:10.1007/s10236-010-0367-2

Литература

1. *Vasilkov A.P.*, *Goldin Yu.A.*, *Gureev B.A.*, *Hoge F.E.*, *Swift R.N.*, *Wright C.W.* Airborne polarized lidar detection of scattering layers in the ocean // Applied Optics. 2001. Vol. 40, N 24. P. 4353–4364. doi:10.1364/AO.40.004353
2. *Churnside J.H.*, *Donaghay P.L.* Thin scattering layers observed by airborne lidar // ICES Journal of Marine Science. 2009. Vol. 66, N4. P. 778–789. doi:10.1093/icesjms/fsp029
3. *Collister B.L.*, *Zimmerman R.C.*, *Hill V.J.*, *Sukenik C.I.*, *Balch W.M.* Polarized lidar and ocean particles: insights from a mesoscale coccolithophore bloom // Applied Optics. 2020. Vol. 59, N 15. P. 4650–4662. doi:10.1364/AO.389845
4. *Churnside J.H.*, *Brown E.D.*, *Parker-Stetter S.*, *Horne J.K.*, *Hunt G.L.*, *Hillgruber N.*, *Sigler M.F.*, *Vollenweider J.J.* Airborne remote sensing of a biological hot spot in the southeastern Bering Sea // Remote Sensing. 2011. Vol. 3, N 3. P. 621–637. doi:10.3390/rs3030621
5. *Goldin Y.A.*, *Vasilev A.N.*, *Lisovskiy A.S.*, *Chernook V.I.* Results of Barents Sea airborne lidar survey // Proceedings SPIE. Current Research on Remote Sensing, Laser Probing, and Imagery in Natural Waters (13 April 2007). 2007. Vol. 6615. P. 126–136. doi:10.1117/12.740456
6. *Zhong C.*, *Chen P.*, *Pan D.* An Improved Adaptive Subsurface Phytoplankton Layer Detection Method for Ocean Lidar Data // Remote Sensing. 2021. Vol. 13, N 19. P. 3875. doi:10.3390/rs13193875
7. *Churnside J.H.*, *Ostrovsky L.A.* Lidar observation of a strongly nonlinear internal wave train in the Gulf of Alaska // International Journal of Remote Sensing. 2005. Vol. 26, N 1. P. 167–177. doi:10.1080/01431160410001735076
8. *Bukin O.A.*, *Major A.Y.*, *Pavlov A.N.*, *Shevtsov B.M.*, *Kholodkevich E.D.* Measurement of the lightscattering layers structure and detection of the dynamic processes in the upper ocean layer by shipborne lidar // International Journal of Remote Sensing. 1998. Vol. 19, N 4. P. 707–715. doi:10.1080/014311698215946

9. *Глухов В.А.*, *Гольдин Ю.А.*, *Родионов М.А.* Лидарный метод регистрации внутренних волн в водах с двухслойной стратификацией гидрооптических характеристик // Фундаментальная и прикладная гидрофизика. 2021. Т. 14, № 3. С. 86–97. doi:10.7868/S2073667321030084
10. *Hoge F.E.*, *Wright C.W.*, *Krabill W.B.*, *Buntzen R.R.*, *Gilbert G.D.*, *Swift R.N.*, *Berry R.E.* Airborne lidar detection of subsurface oceanic scattering layers // Applied Optics. 1988. Vol. 27, N 19. P. 3969–3977. doi:10.1364/AO.27.003969
11. *Goldin Y.A.*, *Gureev B.A.*, *Ventskut Y.I.* Shipboard polarized lidar for seawater column sounding // Proccedings SPIE. Current Research on Remote Sensing, Laser Probing, and Imagery in Natural Waters (13 April 2007). 2007. Vol. 6615. P. 152–159. doi:10.1117/12.740466
12. *Гольдин Ю.А.*, *Гуреев Б.А.*, *Родионов М.А.*, *Глухов В.А.* Морской поляризационный лидар ПЛД-1 // Труды XIII Всероссийской конференции «Прикладные технологии гидроакустики и гидрофизики» (Санкт-Петербург, 2016). Санкт-Петербург: Федеральное государственное бюджетное учреждение науки Санкт-Петербургский научный центр РАН, 2016. С. 215–217.
13. *Глухов В.А.*, *Гольдин Ю.А.*, *Родионов М.А.* Экспериментальная оценка возможностей лидара ПЛД-1 по регистрации гидрооптических неоднородностей в толще морской среды // Фундаментальная и прикладная гидрофизика. 2017. Т. 10, № 2. С. 41–48. doi:10.7868/S207366731702006X
14. *Goldin Yu.A.*, *Rogozkin D.B.*, *Sheberstov S.V.* Polarized Lidar Sounding of Stratified Seawater // Proceedings of IV International Conference “Current Problems in Optics of Natural Waters (ONW’2007)”. Nizhny Novgorod, 2007. P. 175–178.
15. *Химченко Е.Е.*, *Серебряный А.Н.* Внутренние волны на Кавказском и Крымском шельфах Черного моря (по летне-осенним наблюдениям 2011–2016 гг.) // Океанологические исследования. 2018. Т. 46, № 2, С. 69–87. doi:10.29006/1564–2291.JOR-2018.46(2).7
16. *Серебряный А.Н.*, *Иванов В.А.* Исследования внутренних волн в Черном море с океанографической платформы МГИ // Фундаментальная и прикладная гидрофизика. 2013. № 3. С. 34–45.
17. *Зимин А.В.*, *Свергун Е.И.* Анализ характеристик и оценка ожидаемых высот внутренних волн на шельфе Крыма по данным экспедиции летом 2016 года // Труды всероссийской научно-практической конференции «IV Феодосийские научные чтения» (Санкт-Петербург, 11–12 сентября 2017 г.). Феодосия: МБУК ФМД, «Арт-Лайф», 2017. С. 230–234.
18. *Лаврова О.Ю.*, *Серебряный А.Н.*, *Митягина М.И.*, *Бочарова Т.Ю.* Подспутниковые наблюдения мелкомасштабных гидродинамических процессов в северо-восточной части Черного моря // Современные проблемы дистанционного зондирования Земли из космоса. 2013. Т. 10, № 4. С. 308–322.
19. *Иванов В.А.*, *Шульга Т.Я.*, *Багаев А.В.*, *Медведева А.В.*, *Пластун Т.В.*, *Вержевская Л.В.*, *Свищева И.А.* Внутренние волны на шельфе Черного моря в районе Гераклейского полуострова: моделирование и наблюдение // Морской гидрофизический журнал. 2019. Т. 35, № 4. doi:10.22449/0233-7584-2019-4-322-340
20. *Астафьева Н.М.* Вейвлет-анализ: основы теории и примеры применения // Успехи физических наук. 1996. Т. 166, № 11. С. 1145–1170. doi:10.3367/UFNr.0166.199611a.1145
21. *Жегулин Г.В.* Использование вейвлет-анализа для оценки связи гидрологических и гидрооптических колебаний в диапазоне внутренних волн по данным натурных наблюдений в Белом море // Фундаментальная и прикладная гидрофизика. 2016. Т. 9, № 3. С. 48–56.
22. *Press W.H.*, *Teukolsky S.A.* Savitzky–Golay smoothing filters // Computers in Physics. 1990. Vol. 4, N 6. P. 669–672. doi:10.1063/1.4822961
23. *Короновский А.А.*, *Храмов А.Е.* Непрерывный вейвлетный анализ и его приложения. М.: ФИЗМАТЛИТ, 2003. 176 с.
24. *Huang N.E.*, *Wu Z.* A review on Hilbert-Huang transform: Method and its applications to geophysical studies // Reviews of Geophysics. 2008. Vol. 46, N 2. doi:10.1029/2007RG000228
25. *Навроцкий В.В.*, *Ляпидевский В.Ю.*, *Павлова Е.П.*, *Храпченков Ф.Ф.* Внутренние волны и перемешивание в шельфовой зоне моря // Известия ТИНРО (Тихоокеанского научно-исследовательского рыбохозяйственного центра). 2010. Т. 162. С. 324–337.

26. *Навроцкий В.В.*, *Лобанов В.Б.*, *Сергеев А.Ф.*, *Воронин А.А.*, *Горин И.И.*, *Павлова Е.П.* Динамическая структура каскадинга в заливе Петра Великого (Японское море) // Океанологические исследования. 2020. Т. 48, № 3. С. 148–163. doi:10.29006/1564–2291.JOR-2020.48(3).9
27. *Dätig M.*, *Schlurmann T.* Performance and limitations of the Hilbert–Huang transformation (HHT) with an application to irregular water wave // Ocean Engineering. 2004. Vol. 31, N 14–15. P. 1783–1834. doi:10.1016/j.oceaneng.2004.03.007
28. *Ezer T.*, *Heyman W.D.*, *Houser C.*, *Kjerfve B.* Modeling and observations of high-frequency flow variability and internal waves at a Caribbean reef spawning aggregation site // Ocean Dynamics. 2010. Vol. 61, N 5. P. 581–598. doi:10.1007/s10236-010-0367-2

About the Authors

Vladimir A. Glukhov	Scientist, Shirshov Institute of Oceanology, Russian Academy of Sciences, 36 Nakhimovsky Prosp., Moscow, 117997, Russia, ROR 00n1e1p60	ORCID ID: 0000-0003-4555-8879, WoS ResearcherID: GSD-4886-2022, Scopus AuthorID: 57191414331, elibrary AuthorID: 916467, e-mail: vl.glukhov@inbox.ru
Yuriy A. Goldin	PhD. (Phys.-Math.Sci.), Leading scientist, Shirshov Institute of Oceanology, Russian Academy of Sciences, 36 Nakhimovsky Prosp., Moscow, 117997, Russia, ROR 00n1e1p60, ROR 00n1e1p60	ORCID ID: 0000-0001-5731-5458, Scopus AuthorID: 6602648464, elibrary AuthorID: 58653, e-mail: goldin@ocean.ru
Gleb V. Zhegulin	Scientist, Shirshov Institute of Oceanology, Russian Academy of Sciences, 36 Nakhimovsky Prosp., Moscow, 117997, Russia, ROR 00n1e1p60	ORCID ID: 0000-0002-8762-0899, WoS ResearcherID: AAP-7395-2021, Scopus AuthorID: 57195070290, elibrary AuthorID: 768992, e-mail: gleb-jegulin@rambler.ru
Maxim A. Rodionov	PhD. (Phys.-Math.Sci.), Leading scientist, Shirshov Institute of Oceanology, Russian Academy of Sciences, 36 Nakhimovsky Prosp., Moscow, 117997, Russia, ROR 00n1e1p60, ROR 00n1e1p60	ORCID ID: 0000-0002-7397-0548, Scopus AuthorID: 56034199200, elibrary AuthorID: 203807, e-mail: maxim_rodionov@mail.ru